

Generation of Supraclusters and Nanoclusters Using Laser Desorption/Ionisation Mass Spectrometry

Paul J. Dyson,^{1,4} John E. McGrady,¹ Meike Reinhold,¹
Brian F. G. Johnson,² J. Scott McIndoe,² and
Patrick R. R. Langridge-Smith³

Received November 15, 1999

Laser desorption/ionisation of discrete molecular clusters combined with time-of-flight (TOF) or Fourier-transform ion cyclotron resonance (FTICR) mass spectrometry affords spectra in which extensive higher mass clusters are observed. The size of the largest cluster aggregates (or supraclusters) is of the same order of magnitude as nanoclusters. The spectra obtained using TOF mass spectrometry sometimes exhibit post-source decay fragmentation, depending upon the operational conditions employed during data acquisition, which, although providing useful data on the ligand dissociation dynamics, complicate spectral interpretation. Complementary FTICR mass spectra are free of such features. The identities of the supra/nanoclusters generated from the molecular cluster precursors have not been conclusively established but are mostly coordinatively unsaturated. Density functional molecular orbital calculations have identified the possible structures of the comparatively simple electronically unsaturated system, $[\text{Ru}_3(\text{CO})_6]^-$, that provides a clue to the aggregation mechanism.

KEY WORDS: Rhodium; ruthenium; osmium; carbonyl; cluster; mass spectrometry.

INTRODUCTION

Mass spectrometry has been widely employed by cluster chemists to facilitate the characterisation of novel clusters prepared in the laboratory [1–3]. Of the two most favoured ionisation techniques currently used in

¹ Department of Chemistry, The University of York, Heslington, York YO10 5DD, UK.

² Department of Chemistry, The University of Cambridge, Lensfield Road, Cambridge CB2 1EW, UK.

³ Department of Chemistry, The University of Edinburgh, West Mains Road, Edinburgh EH9 3JJ, UK.

⁴ To whom correspondence should be addressed.

mass spectrometry, viz. electrospray and laser desorption, only the former has been applied to routinely determine the molecular weight of clusters [3–5]. Although laser desorption/ionisation is ideally suited to solid substrates with low volatilities and high molecular weights [6], it has not been widely applied to cluster substrates due to the complicated gas-phase reactions which take place in the mass spectrometer, making interpretation of the resulting spectra far more involved [7–12]. In this paper we summarise some of our results in this area and illustrate the complications that routinely arise. We also propose a possible mechanism for the cluster aggregation process and suggest how it should be possible to harness lasers to produce nanoclusters on a preparative scale.

RESULTS AND DISCUSSION

Our initial studies on the characterisation of ruthenium clusters using laser desorption/ionisation time-of-flight mass spectrometry (LDI-TOF-MS) led to the detection of clusters containing large numbers of ruthenium atoms (up to ca. 300) [7, 8]. These so-called supraclusters or nanoclusters were generated from molecular cluster precursors with nuclearities of four and six. The relatively low resolution of the instruments used in these early experiments, combined with the natural isotope composition of ruthenium, prevented detailed assignment. Since most attention was focussed on $\text{Ru}_6\text{C}(\text{CO})_{17}$ [8] we decided to investigate the related octahedral rhodium cluster $\text{Rh}_6(\text{CO})_{16}$ as rhodium comprises a single isotope. In addition, instruments capable of higher resolution were also used.

Time-of-Flight Mass Spectra

The LDI-TOF mass spectrum of $\text{Rh}_6(\text{CO})_{16}$ exhibited the same type of carbonyl loss and aggregation phenomena as $\text{Ru}_6\text{C}(\text{CO})_{17}$ [8] although clustering does not extend to such high masses under the conditions employed. A typical negative ion spectrum for $\text{Rh}_6(\text{CO})_{16}$ is shown in Fig. 1. There are ten distinct peak envelopes, which correspond to clusters with nuclearities ranging from 6 to 60, as indicated in the figure (also see Table I). Clustering beyond 60 rhodium atoms is observed but the relative intensities of the peaks are very low. Clustering takes place in multiples of six, suggesting that the Rh_6 core present in the precursor cluster remains intact during the laser ablation process. The initial desorption/ionisation process causes CO loss to occur from the cluster precursor and cluster fragmentation is not observed. In the parent region peaks corresponding to $\text{Rh}_6(\text{CO})_{16-x}$ ($x=1-10$) are observed and as these clusters become increasingly coordinatively unsaturated they are more likely to undergo

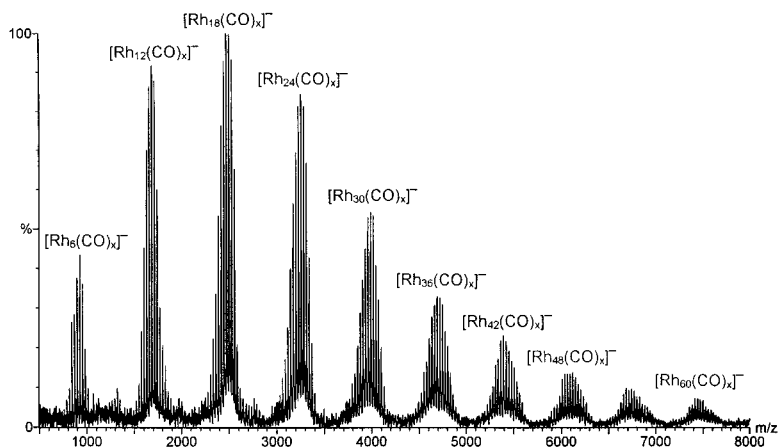


Fig. 1. The negative ion LDI-TOF mass spectrum of $\text{Rh}_6(\text{CO})_{16}$ between 500 and 8000 Da recorded in reflectron mode. Note that each envelope of peaks refers to a range of clusters with the same nuclearity metal core but with different numbers of CO ligands.

aggregation reactions. In addition, the highest mass peak in the parent region of $\text{Rh}_6(\text{CO})_{16}$ is observed at 1037.1 Da and corresponds to $[\text{Rh}_6(\text{CO})_{15}]^-$. Ionisation accompanied by loss of one CO is typical of neutral homoleptic clusters [9] although clusters with other ligands [11] and charged clusters [12] behave differently. The different ionisation mechanisms of various types of clusters clearly complicate the determination of molecular weights of unknown compounds. However, with the exception of charged clusters, derivatisation methods must be used in electrospray mass

Table I. Assignment of the Most Intense Peaks of Each $(\text{Rh}_6)_n$ ($n = 1-10$) Envelope in the Negative Ion LDI-TOF Mass Spectrum of $\text{Rh}_6(\text{CO})_{16}$. Only the Most Intense Peak in Each Envelope Is Listed

Assigned ion	Obs.	Obs. PSD	Calc.
$[\text{Rh}_6(\text{CO})_{11}]^-$	925.5	928.5	925.4
$[\text{Rh}_{12}(\text{CO})_{16}]^-$	1683.4	1686.6	1682.8
$[\text{Rh}_{18}(\text{CO})_{23}]^-$	2496.8	2499.3	2496.2
$[\text{Rh}_{24}(\text{CO})_{28}]^-$	3256	3259	3253.6
$[\text{Rh}_{30}(\text{CO})_{32}]^-$		3989	3983.0
$[\text{Rh}_{36}(\text{CO})_{36}]^-$		4720	4712.4
$[\text{Rh}_{42}(\text{CO})_{39}]^-$		5421	5413.8
$[\text{Rh}_{48}(\text{CO})_{42}]^-$		6123	6115.3
$[\text{Rh}_{54}(\text{CO})_{42}]^-$		6740	6732.7
$[\text{Rh}_{60}(\text{CO})_{45}]^-$		7442	7434.1

spectrometry, where simple ionisation processes do not take place, to determine molecular weights of these types of compounds [5].

The spectrum shown in Fig. 1 is typical of both negative and positive ion spectra although in general negative ions give rise to aggregation products extending to higher masses and with higher intensities than the positive ions. From a synthetic viewpoint cluster growth requires reductive conditions and this environment is more likely to be mimicked in the mass spectrometer when operated in negative mode.

The gross features of the spectra are the same whether the instrument is operated in linear or reflectron mode. However, close inspection of each envelope of peaks reveals significant differences between the spectra recorded in the two operational modes and these differences can be appreciated from Fig. 2, which shows the Rh_{12} envelope recorded in linear and reflectron mode. A single peak is observed for each ion in the linear spectrum with relatively low resolution (ca. a factor of four) compared to the reflectron spectrum. Peak assignments are listed in Table I. The broad signals obtained when the instrument is operated in linear mode is due to the fact that ions with the same m/z ratio have a large range of internal energies which broadens their flight times through the flight tube. So-called time focusing (and hence mass focusing, since mass is directly proportional to

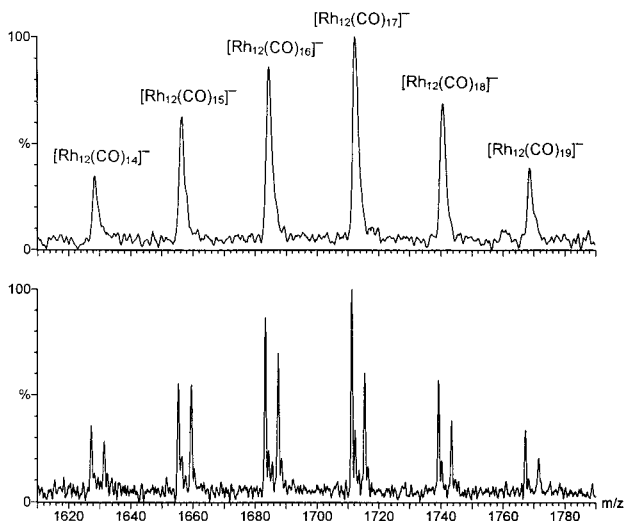


Fig. 2. The negative ion LDI-TOF mass spectrum of $\text{Rh}_6(\text{CO})_{16}$ showing the $[\text{Rh}_{12}(\text{CO})_x]^-$ ($x = 14-19$) ions recorded in linear mode (top) and reflectron mode (bottom). Note the higher resolution of the peaks when the data is acquired in reflectron mode together with the presence of metastable ions.

time in a TOF instrument) using a reflectron significantly improves the resolution (Fig. 2b) as evident from the narrower widths of the peaks. The reflectron focuses the ions by equilibrating the energies of particles with the same m/z value. However, while the resolution increases, additional peaks appear. These peaks are due to metastable species also known as post source decay fragments that are produced in the flight tube once the ions have left the source. The cluster ions generated during the laser ablation process have high internal energies. The ions with the highest internal energies instantaneously eject neutral CO molecules and some undergo further reaction in the high density desorption plume immediately after laser ablation to form the cluster aggregate ions. The cluster ions cool through these processes but some continue to eject carbonyls when in the flight tube of the mass spectrometer. In the linear process these metastable peaks arrive at approximately the same times as their parent ions and are therefore not observed. Fragments formed in the flight tube of a reflectron instrument arrive at a different time to the parent ions. The difference arises because the ions are reflected by an electric field and the parent and daughter ions penetrate the field to different levels and it is this process which gives rise to the secondary set of peaks (as well as other sets in certain cases). The extent of post source decay increases with the size of the cluster and for the very large clusters the real ions are often not even observed and all the peaks correspond to post source decay fragments which makes peak assignments extremely difficult. It is possible to estimate the size of the parent ions from which the daughter ion peaks were derived [13] and we are currently analysing the data in detail to establish this information which will be the subject of a future report. The actual mass difference between the true peak and the metastable peak depends on many parameters including the actual type of reflectron device used (which varies from instrument to instrument), the potentials and field regions etc. The effect of the metastable peaks can also be seen in Fig. 1 where they shift the centre of each main peak envelope to slightly higher mass. Caution should always be applied to the interpretation of spectra of these types of compounds recorded in this way.

Fourier-Transform Ion Cyclotron Resonance Mass Spectra

FTICR mass spectrometry has been shown to lead to cluster aggregation products that can be unambiguously assigned due to the extremely high resolution that may be achieved [14–17]. We have recently recorded the negative ion LDI-FTICR mass spectra of several clusters, including $\text{Os}_3(\text{CO})_{12}$, which shows features related to the LDI-TOF spectra. The main advantage is that the resolution allows complete assignments of all

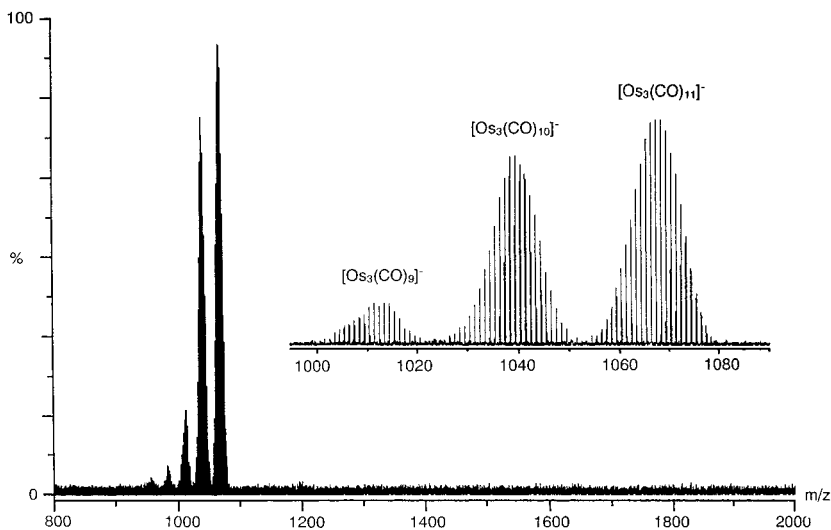


Fig. 3. The negative ion LDI-FTICR mass spectrum of $\text{Os}_3(\text{CO})_{12}$ in the parent ion region. The clean baseline observed arises as the data was acquired between 900 and 1100 Da. Only a small mass range is collected at any one time to maximise resolution. Note the narrow peaks and baseline resolution in the expanded region between 1000 and 1080 Da.

the peaks. Furthermore, processes such as post-source decay do not take place and fragments ions may be selected, trapped and reacted further.

Figure 3 shows the parent cluster region, and, as in the TOF spectra, the highest mass peak observed corresponds to the parent ion less one CO ligand, viz. $[\text{Os}_3(\text{CO})_{11}]^-$. The full natural isotope fingerprint is fully resolved and corresponds to a triosmium species. Cluster aggregates are also formed with a wide range of nuclearities including a very strong peak which corresponds to an osmium cluster with a nuclearity of 12. Despite many conventional synthetic studies producing a large number of homoleptic clusters of osmium with nuclearities between 3 and 20 [18], as far as we are aware no homoleptic dodecaosmium cluster has been reported.

Mechanistic Inferences

The structures of the clusters produced in the LDI experiments remain a matter of speculation, but application of electron counting methods [19] reveals that the vast majority of species are coordinatively unsaturated. The supraclusters containing in the order of 50 metals and above could be described as nanoclusters, and we intend to mimic the conditions of the laser desorption process on a synthetic scale using various isolation methods in order to try and obtain macroscopic quantities of these nanoclusters.

Related experiments have been conducted previously [20], but insights acquired from LDI mass spectrometry (in particular tandem mass spectrometry using FTICR instruments) should provide useful information that may provide greater control of the masses of the nanoclusters obtained.

Under certain conditions the negative ion LDI-TOF mass spectra of $M_3(\text{CO})_{12}$ ($M = \text{Ru}$ and Os) can be tuned so that complete stripping of the carbonyl ligands from the trimetal cluster can be obtained. Under such conditions it has been found that a peak corresponding to the $[\text{M}_3(\text{CO})_6]^-$ ion dominates. The electronic structure of this carbonyl deficient cluster has been investigated with density functional molecular orbital calculations. The structures and electronic properties of stable metal carbonyl clusters have been the topic of much debate. The mobility of carbonyl ligands is well documented [21], and as a result, several minima are often located on the potential energy hypersurface of a cluster, corresponding to different distributions of ligands around the metal core. The bonding within the metal core itself, however, tends to be relatively independent of the ligand positions, and the structures can, at least in the case of bi- and trinuclear clusters, be rationalised in terms of the 18-electron rule. For example, the triangular structure of $\text{Ru}_3(\text{CO})_{12}$ arises from the formation of two Ru–Ru single bonds which completes the 18-electron configuration about each metal centre. High level calculations, mostly performed using approximate density functional theory, have served to confirm this simple model in a number of cases [22]. More recently, attention has turned to the species formed when one or more CO ligand is lost from the stable metal clusters. In these highly reactive systems, structural analysis using conventional methods is clearly not possible, and computational chemistry represents the only source of geometric information. In the past three years, approximate density functional theory has been used to study the relative stabilities of various isomers of $\text{Mn}_2(\text{CO})_x$ ($x=9$ [23] and 8 [24]), $\text{Fe}_2(\text{CO})_8$ [25], and $\text{Cp}_2\text{Fe}_2(\text{CO})_x$ ($x=2, 3$) [26]. In each case, the loss of a carbonyl ligand causes a contraction of the metal–metal bond, consistent with an increase in formal bond order.

The relative stabilities of isomers of $[\text{Ru}_3(\text{CO})_6]^-$, the dominant species observed in the LDI-FT-ICR spectrum of $\text{Ru}_3(\text{CO})_{12}$, differs from those described above in the extreme degree of its electron deficiency (11 electrons less than its neutral, saturated precursor). The structures of the four most stable isomers located on the potential energy surface of $[\text{Ru}_3(\text{CO})_6]^-$ are shown in Fig. 4. The three most stable structures share a common six-membered $\text{Ru}_3(\mu\text{-CO})_3$ core in a chair conformation, the only difference between **1**, **2**, and **3** being the distribution of the remaining three terminal CO groups. In **1** two are equatorial and one axial, in **2** all three are equatorial and in **3**, two are axial and one equatorial (the fourth

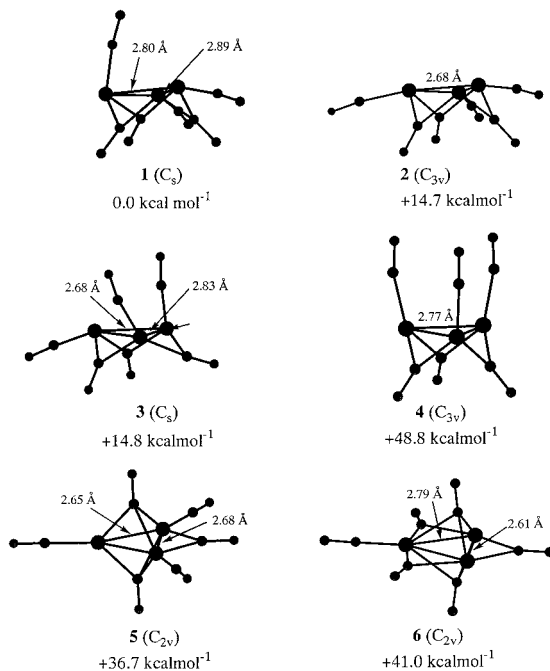


Fig. 4. Structures of $[\text{Ru}_3(\text{CO})_6]^-$ calculated using density functional theory.

permutation, **4**, with all three terminal carbonyls axial, is 49 kcal/mol⁻¹ less stable due to repulsions between the axial CO groups). More compact structures such as **5** and **6**, with two face-capping CO ligands, are also substantially less stable, lying approximately 40 kcal/mol⁻¹ above **1**. In all cases there is a substantial contraction of the Ru–Ru bonds relative to 2.94 Å, the corresponding value for a Ru–Ru single bond in $\text{Ru}_3(\text{CO})_{12}$, consistent with the emergence of some unsaturated character in the metal–metal bonds.

The identification of the most stable isomers of $[\text{Ru}_3(\text{CO})_6]^-$ allow us to make some suggestions as to possible mechanisms for cluster growth. The calculations indicate that, in the gas phase, the cluster fragment will contain a chair-shaped $\text{Ru}_3(\mu\text{-CO})_3$ core, with three terminal CO ligands making up the remainder of the coordination sphere. These ligands are likely to be highly mobile, and so substantial concentrations of **1**, **2**, and **3** will be present in the reaction mixture. Isomer **2** is particularly noteworthy, as in this case all six CO ligands lie on one side of the Ru_3 triangle, leaving the opposite face exposed. This configuration, in conjunction with the partial unsaturation of the Ru–Ru bonds, will make isomer **2** highly

susceptible to attack by other $\text{Ru}_x(\text{CO})_y$ fragments present in the spectrometer, leading to the cluster aggregation phenomena observed in the LDI-FT-ICR experiment. Further work is currently underway to investigate the detailed nature of the bonding in the electron-deficient $[\text{Ru}_3(\text{CO})_6]^-$ cluster, as well as establishing the structures of other unsaturated species, $[\text{Ru}_3(\text{CO})_x]^-$ ($x = 11-0$).

With the hexanuclear clusters a similar type of mechanism can be envisaged involving aggregation of intact cluster cores. However, with the trinuclear clusters aggregation does not occur in simple multiples of three but clusters are observed for each integer. It is not clear, for example, whether a tetranuclear cluster is formed from aggregation of a trinuclear and mononuclear or two dinuclear species, or from expulsion of two metal fragments from a hexanuclear cluster. We hope that FTICR-MS experiments will help to delineate the precise mechanism.

Concluding Comments

All the neutral transition metal carbonyl clusters we have investigated so far show aggregation, and since the range of precursor compounds is vast (a number of transition metal clusters are even commercially available), the potential for studying a wide range of gas-phase clusters over a range of nuclearities is enormous. There is also the possibility of using discrete molecular clusters as a simple source of gas phase clusters for conducting gas-phase coordination chemistry. By analogy to the work of Kroto and others, who initially observed a peak in a mass spectrum which corresponded to C_{60} and later isolated the molecule in the laboratory, it might be possible to isolate the clusters and nanoclusters produced in these experiments.

EXPERIMENTAL

Instrumentation and Sample Handling

LDI-TOF spectra were recorded on a Micromass TOFSpec-2E instrument equipped with a standard 337 nm N_2 laser. FTICR spectra were recorded on an IonSpec UltimaTM FTMS instrument operated at 4.7 T, using an IonSpec OMEGATM data system. Laser desorption/ionisation was performed with a Lambda Physik model EMG 201MSC excimer laser operating on the xenon fluoride line at 353 nm. Samples were deposited onto a stainless steel probe from dichloromethane solution.

Density Functional Calculations

All calculations were performed using the Amsterdam Density Functional (ADF) package, version 2.3 [27, 28]. The local density approximation

was used (Vosko, Wilk, and Nusair [29] parameterisation), along with the gradient corrections to exchange (Becke) [30] and correlation (Perdew) [31]. All calculations were performed in a spin-restricted manner. The Ru atoms were described using a triple- ζ basis set, while a double- ζ basis with a single polarisation function was used for C and O. Geometries were optimised using the gradient algorithm of Ziegler and Versluis [32].

ACKNOWLEDGMENTS

We would like to thank the Royal Society for a University Research Fellowship (PJD) and the New Zealand Foundation for Science and Technology for a Postdoctoral Fellowship (JSM, contract CAM801). We would also like to thank Glen Critchley (Micromass) and Yunzhi Li (IonSpec) for help collecting the data.

REFERENCES

1. R. Cotter and C. Fenslau (1987). *Chem. Rev.* **87**, 501.
2. R. Colton, A. DiAgostine, and J. C. Traeger (1995). *Mass Spectrom. Rev.* **14**, 79.
3. B. F. G. Johnson and J. S. McIndoe, *Coord. Chem. Rev.*, in press.
4. W. Henderson, J. S. McIndoe, B. K. Nicholson, and P. J. Dyson (1996). *Chem. Commun.* 1183.
5. W. Henderson, J. S. McIndoe, B. K. Nicholson, and P. J. Dyson (1998). *J. Chem. Soc. Dalton Trans.* 519.
6. F. Hillenkamp, M. Karas, R. C. Beavis, and B. T. Chait (1991). *Anal. Chem.* **63**, 1193.
7. M. J. Dale, P. J. Dyson, B. F. G. Johnson, C. M. Martin, P. R. R. Langridge-Smith, and R. Zenobi (1995). *J. Chem. Soc. Chem. Commun.* 1689.
8. M. J. Dale, P. J. Dyson, B. F. G. Johnson, P. R. R. Langridge-Smith, and H. T. Yates (1996). *J. Chem. Soc. Dalton Trans.* 774.
9. G. Critchley, P. J. Dyson, B. F. G. Johnson, J. S. McIndoe, R. K. O'Reilly, and P. R. R. Langridge-Smith (1999). *Organometallics* **18**, 4090.
10. W. J. Dollard, P. J. Dyson, T. Jackson, B. F. G. Johnson, J. S. McIndoe, and P. R. R. Langridge-Smith (1999). *Inorg. Commun.* **2**, 587.
11. P. J. Dyson, A. K. Hearley, B. F. G. Johnson, J. S. McIndoe, and P. R. R. Langridge-Smith (1999). *Inorg. Commun.*, in press.
12. P. J. Dyson, A. K. Hearley, B. F. G. Johnson, J. S. McIndoe, and P. R. R. Langridge-Smith, *Inorg. Chem.* **2**, 591.
13. For example, see (a) S. Jespersen, P. Chaurand, F. J. C. van Strien, B. Spengler, and J. van der Greef (1999). *Anal. Chem.* **71**, 660. (b) J. Vinh, D. Loyaux, V. Redeker, and J. Rossier (1997). *Anal. Chem.* **69**, 3979.
14. J. Wonka and D. P. Ridge (1984). *J. Am. Chem. Soc.* **106**, 67.
15. D. A. Fredeen and D. H. Russell (1987). *J. Am. Chem. Soc.* **109**, 3903.
16. S. L. Mullen and A. G. Marshall (1988). *J. Am. Chem. Soc.* **110**, 1766.
17. W. K. Meckstroth and D. P. Ridge (1984). *Int. J. Mass Spec. and Ion Proc.* **106**, 4307.
18. J. Lewis and P. R. Raithby (1995). *J. Organomet. Chem.* **500**, 227.
19. M. S. Owen (1988). *Polyhedron* **7**, 253.

20. G. H. Lee, S. H. Huh, and H. I. Jung (1998). *J. Mol. Struc.* **440**, 141.
21. B. F. G. Johnson (1997). *J. Chem. Soc. Dalton Trans.* 1473.
22. A. Rosa, G. Ricciardi, E. J. Baerends, and D. J. Stufkens (1995). *Inorg. Chem.* **34**, 3425.
23. A. Rosa, G. Ricciardi, E. J. Baerends, and D. J. Stufkens (1996). *Inorg. Chem.* **35**, 2886.
24. T. A. Barckholtz and B. E. Bursten (1998). *J. Am. Chem. Soc.* **120**, 1926.
25. H. Jacobsen and T. Ziegler (1996). *J. Am. Chem. Soc.* **118**, 4631.
26. M. Vitale, M. E. Archer, and B. E. Bursten (1998). *Chem. Commun.* 179.
27. E. J. Baerends, D. E. Ellis, and P. Ros (1973). *Chem. Phys.* **2**, 41.
28. G. te Velde and E. J. Baerends (1992). *J. Comp. Phys.* **99**, 84.
29. J. Vosko, M. Wilk, and M. Nussair (1980). *Can. J. Phys.* **58**, 1200.
30. A. Becke (1988). *Phys. Rev. A* **38**, 3098.
31. J. P. Perdew (1986). *Phys. Rev. B* **34**, 7406.
32. T. Ziegler and L. Versluis (1988). *J. Chem. Phys.* **88**, 322.